Vol. **111** (2007) *ACTA PHYSICA POLONICA A* No. 6

Proceedings of the XII National School "Correlated Electron Systems...", Ustroń 2006

Local Magnetic and Electronic Properties of the $A_2FeM'O_6$ (A = Ba, Sr, Ca, M′ = Mo, Re) Double Perovskites

D. Zając[a], M. Sikora[a], V. Prochazka[a], M. Borowiec[a], J. Stępień[a], Cz. Kapusta[a,*], P.C. Riedi[b], C. Marquina[c], J.M. De Teresa[c,d] and M.R. Ibarra[c,d]

[a]Faculty of Physics and Applied Computer Science
AGH University of Science and Technology
al. Mickiewicza 30, 30-059 Kraków, Poland
[b]Department of Physics & Astronomy, University of St. Andrews
St. Andrews, Fife, KY16 9SS, Scotland, UK
[c]Universidad de Zaragoza-CSIC, Facultad de Ciencias
Pedro Cerbuna 12, Zaragoza 50009, Spain
[d]Instituto de Nanociencia de Aragon, Universidad de Zaragoza (INA)
Pedro Cerbuna 12, Zaragoza 50009, Spain

Dedicated to Professor Józef Spałek on the occasion of his 60th birthday

The results of a combined NMR, X-ray absorption spectroscopy and X-ray magnetic circular dichroism study of the $AA'FeMoO_6$ and $AA'FeReO_6$ double perovskites are presented. They revealed a dependence of electronic and magnetic properties, including a d-electron transfer between Fe and Mo sites, on the structural tolerance factor. The maximum value of the $4d$ Mo electron occupation and the corresponding Mo moment is obtained for the tolerance factor of unity. This corresponds to the maximum strength of the magnetic interaction and, respectively, to the Curie temperature. The dominant $T^{5/2}$ type temperature dependence of the Mo hyperfine field reveals the half-metallicity of the $AA'FeMoO_6$ compounds. Antisite defects and antiphase boundaries have been identified in NMR measurements and the strength of their magnetic coupling have been determined. A considerable orbital contribution to the Re and Fe magnetic moments were found in the NMR and X-ray magnetic circular dichroism measurements on the $AA'FeReO_6$ compounds. Its magnitude decreases with increasing structural tolerance factor and is correlated with their magnetic anisotropy.

PACS numbers: 75.30.–m, 76.60.–k, 76.60.Jx, 78.70.Dm

*corresponding author; e-mail: kapusta@agh.edu.pl

1. Introduction

Double perovskites (DP) of a general formula $A_2MM'O_6$, where A is an alkaline earth, and M and M′ are 3*d*, 4*d*, and/or 5*d* transition metals belong to a very broad family of oxide compounds crystallising in the perovskite structure. They exhibit intriguing magnetic and electronic properties including half metallicity, a considerable low field magnetoresistance (LFMR) and a variety of magnetic structures, see review paper [1]. Magnetic and electronic properties are closely interrelated, due to the same (*d*) character of the "magnetic" and "conduction" electrons. Exchange interactions can occur between ions of the same element, as e.g. in manganese perovskites, as well as between ions of different elements, as e.g. in double perovskites. The interplay of lattice, charge, and spin degrees of freedom causes a variety of electronic and magnetic properties ranging from a metallic ferro- or ferrimagnetism to antiferromagnetic or paramagnetic insulating behaviour. This also brings about the magnetoresistive properties of the compounds.

The interplay between magnetic and electronic transport properties in these systems can be controlled by substitution of alkaline earths (e.g. Ba, Sr, Ca) or lanthanides (e.g. La, Pr, Nd) in the A-site, as well as by the substitution of transition metals (e.g. Fe, Cr, Mn, Mo, Rh, Ru, W, Re). Among the double perovskites, the Fe–Mo and Fe–Re compounds, which are the subject of the study presented in this paper, have recently attracted a great deal of interest among the researchers. Their relatively high magnetic ordering temperature (in most cases higher than the room temperature) compared to that of manganese perovskites, and a significant LFMR make them especially interesting for applications, e.g. in magnetoelectronics or spintronics. The LFMR is explained in terms of intergranular tunneling MR (ITMR), and is related to the half-metallic nature of the ground state of the compound. This half-metallic character and the high degree of spin polarization of the charge carriers are also very important for the technical applications of the DP.

In their crystal structure the oxygen and the large TM cations are close packed, whereas M and M′ are located inside the oxygen octahedra. The arrangement of the M and M′ octahedra is alternating for M and M′ elements with a large difference of ionic radii [2, 3]. In the case of a small difference of M and M′ elements ionic radii, a random distribution of M and M′ occurs [4]. Nevertheless, as the studies carried out on doped compounds conclude, not only the TM cation size but also its valence state determine the M and M′ order in the perovskite structure [5, 6, 4]. The arrangement of the M and M′ octahedra influences the M–O–M′, M–O–M, or M′–O–M′ exchange interactions, and therefore it is very important for understanding the structural, magnetic, and electronic properties of the compounds.

Due to the above mentioned factors, double perovskites can exhibit a variety of crystallographic structures for different alkaline and transition metal ions. The structure at room temperature (RT) can be: cubic — $Fm\bar{3}m$ as for exam-

ple Sr_2FeMoO_6 [7], Ba_2FeMoO_6 [8, 2]; tetragonal — $I4/mmm$ as in the case of Sr_2FeMoO_6 [9]; monoclinic — $P2_1/n$: Ca_2FeMoO_6 [8]. The discrepancies between different authors concerning the crystallographic structure of the same compound, e.g. Sr_2FeMoO_6, can be related to small differences in the chemical composition of DP synthesised under different conditions. This can cause differences in the oxygen stoichiometry as well as in the M, M′ ions ordering, and the resultant amount of structural defects [10, 8, 11]. It is worth noting that when $A_2 = Ba_2$ and SrBa, the compounds crystallise in the cubic structure [12]. A decrease in the ionic radius of A when substituting by Sr or Ca leads to a reduction of the symmetry of the unit cell.

For a quantitative characterisation of the symmetry of the lattice, the tolerance factor f is defined, similarly to that in AMO_3 perovskites

$$f = \frac{r_A + r_O}{\sqrt{2}(\langle r_M \rangle + r_O)},$$

where r_A is the average ionic radius of an ion at the A site, $\langle r_M \rangle$ denotes the average ionic radius for the ions at the M, M′ sites and r_O is the ionic radius of the O^{2-} ion ($r_O \approx 1.40$ Å) [13–17]. A deviation of the tolerance factor from the ideal value $f = 1$ can be a measure of the structural mismatch caused by different ionic radii of the A and M, M′ cations. For $f \neq 1$ the strain due to this mismatch is compensated by a tilt and rotation of the oxygen octahedra. This causes a deviation of the M–O–M′ angle from the ideal value of 180°. For $f \in (0.96; 1)$, the structure prefers a tetragonal lattice; for $f \in (1; 1.06)$ the compounds crystallise in a cubic structure; for $f < 0.96$ — a monoclinic lattice [12, 15], and for $f > 1.06$ a hexagonal structure is expected [15]. In the ideal structure, the arrangement of the M and M′ atoms is similar to that in the Na–Cl structure.

Two types of defects have been identified in DP: antisite (AS) and antiphase boundaries (AP). AS defects arise when the M (M′) ions occupy the position of M′ (M) ions. This results in the creation of equal number of the M and M′ sublattice AS defects. A scheme of the ionic arrangement in the presence of AS defects for both sublattices is presented in [18]. The AP boundary defects can be described as a displacement of the ideal structure along the diagonal Fe–Fe (Mo–Mo) plane. The existence of defects is observed in NMR spectra and, indirectly, in the saturation magnetisation values, as will be discussed in the next paragraphs [19–21].

For the description of the relation between the structural and the electronic properties of DP the electronic bandwidth, W, can be used. This is a parameter similar to that introduced for the characterisation of $A_{1-x}A'_xMnO_3$ perovskites and is defined by an empirical formula [22, 23]:

$$W \approx \frac{\cos\theta}{(\langle r_M \rangle + r_O)^{3.5}},$$

where θ is the tilt angle of the M–O–M′ bond: $\theta = \frac{1}{2}(\pi - \langle M{-}O{-}M' \rangle)$.

The distortions of the oxygen octahedra lead to the change of the Fe–O or Mo–O bonds, and to the change of Fe–O–Mo bond angle. The corresponding decrease in the average cation radius decreases the Fe–O–Mo distance [24, 12]. For Fe–Mo double perovskites with $f > 1$ the difference between Fe–O and Mo–O bonds is larger as f increases. It is worth noting that for Ca_2FeMoO_6 and Sr_2FeMoO_6 a difference of Fe–O (or Mo–O) bond distances and Fe–O–Mo angles along z axis and perpendicular to it is observed [12]. The relation between the tolerance factor f and the bandwidth W for the A_2FeMoO_6 (A_2= Ca_2, Sr_2, SrBa, and Ba_2) series shows a maximum at the tolerance factor close to unity, which corresponds to Sr_2FeMoO_6. A remarkable correlation between W and T_C as a function of r_A was observed for this series [12]. The maximum T_C value is observed for Sr_2FeMoO_6, which corresponds to the compound with the largest estimated electronic bandwidth W in the series. Thus, the strength of the magnetic interaction is related to the value of W. As the magnetic properties are determined by the exchange interactions between the d-electrons governing also the electronic transport in the compounds, they are expected to be strongly interrelated to the electronic and structural properties.

The electronic properties of the Fe–Mo and Fe–Re double perovskites have been studied theoretically and experimentally by several authors [25–34]. The calculations of the density of states (DOS) reveal a gap in the majority spin band at the Fermi level. The minority band exhibits a finite DOS at the Fermi level with a strongly hybridized character of the Fe $3d$ (t_{2g}) and Mo $4d$ (t_{2g}) and O $2p$ states [26, 31]. Such a half-metallic ground state arising from the interplay of structural and electronic factors results in the extraordinary magnetoresistive properties and high magnetic ordering temperature of the Fe–Mo double perovskites.

The model of the electronic structure and the dispersion relations were proposed for Sr_2FeMoO_6 by Kobayashi [25] and developed later by Sarma [26]. The model predicts the existence of the Mo magnetic moment and its antiparallel alignment with the Fe moment, through a large interatomic exchange coupling J_{Fe-Mo}. Mo is usually nonmagnetic as the intra-atomic exchange strength, I_{Mo} within the Mo $4d$ manifold is small. However, in the Fe–Mo double perovskites I_{Mo} is an order of magnitude higher [26] and causes a large splitting of the delocalized $4d$ band, which leads to the appearance of a magnetic moment on molybdenum. The band dispersion calculations within the LMTO method for Fe, Mo, and O reveal a splitting of the d states into the t_{2g} and e_g levels. The minority Fe t_{2g} and Mo t_{2g} spin down states cross the Fermi level and are partially occupied, while the Fe e_g and Mo e_g bands remain empty. The majority bands near the Fermi level originate mainly from the Fe d states hybridised with O p states. The electron hopping between states of the same symmetry (Fe and Mo spin down t_{2g}) causes an additional modification of the bare energy levels. This interaction pushes up (down) the Mo t_{2g} spin up (down) state due to the hybridisation with the corresponding Fe states. These opposite shifts of the Mo spin up and spin down

states increase the effective exchange splitting at the Mo site. Additionally, the antiparallel coupling between the Fe and Mo moments related to the modification of the Mo states is crucial for the enhancement of the I_{Mo} and, consequently, for the increase in the T_{C}. A parallel arrangement of the Fe and Mo moments, on the other hand, would result in a decrease in the T_{C} [26].

The Re-based double perovskites are the most promising compounds in terms of high Curie temperature, e.g. 538 K and 635 K in Ca_2FeReO_6 and Sr_2CrReO_6, respectively [35]. They show even larger variety of magnetic and transport properties than those of Mo-based double perovskites due to an additional electron in the spin-down subband and a stronger spin–orbit coupling in heavier Re ion [35–39]. Although the spin moment of the additional electron decreases the bulk magnetic moment from $\approx 4\ \mu_{\mathrm{B}}$ in $AA'FeMoO_6$ to $\approx 3\ \mu_{\mathrm{B}}$ in $AA'FeReO_6$ double perovskites, its influence on the strength of ferromagnetic interaction seems to be weak, since the Curie temperatures of Sr_2FeMoO_6 and Sr_2FeReO_6 are almost identical, i.e. 410 K and 400 K, respectively. Peculiar differences are observed in the evolution of transport properties caused by a decrease in the average ionic radius ($\langle r_{\mathrm{A}} \rangle$) of alkali earth ions. Smaller $\langle r_{\mathrm{A}} \rangle$ ions lead to lattice distortion and lowering of the local symmetry from cubic ($AA' = Ba_2$) to tetragonal ($AA' = Sr_2$) and monoclinic/orthorhombic ($AA' = Ca_2$) in Re/Mo-based compounds. Then, the Mo-based compounds preserve their weak metallicity, whereas Re-based double perovskites of monoclinic symmetry show semiconducting behaviour and undergo a structural transition at low temperatures, which further increases their resistivity [35, 37–39]. The difference in their magnetic properties is especially intriguing. The Re-based double perovskites are magnetically hard [36, 38, 17] and reveal large magneto-elastic effects [40], which can only be explained by a large magnetocrystalline anisotropy due to anisotropy of not fully quenched orbital moment of Re [38]. This assumption is also supported by the results of recent self-consistent local spin density (LSDA) and generalised gradient approximation (GGA) calculations, which revealed a significant value of $m_{\mathrm{L}} = 0.25\ \mu_{\mathrm{B}}$ per Re atom in Sr_2FeReO_6 [30].

The complexity of the double perovskites, related to the presence of many constituent elements as well as to the possible coexistence of different ionic states of the same element, requires the application of "local probe" methods for a proper characterisation and understanding of their properties. The purpose of this work is to present detailed information on local environments, valences, local magnetic order and their modifications with different element substitutions obtained with "local probe" techniques. The main experimental methods chosen for this study are the nuclear magnetic resonance (NMR), X-ray absorption spectroscopy (XAS), and X-ray magnetic circular dichroism (X-MCD). Based on their results an attempt to explain the relation between structural, electronic, and magnetic properties of the AA'_2FeMoO_6 ($AA' = Ca_2$, Sr_2, SrBa, and Ba_2) and $AA'FeReO_6$ double perovskites ($AA' = Ca_2$, SrCa, Sr_2, BaSr, and Ba_2) is undertaken.

Nuclear magnetic resonance is a technique that uses nuclear spins and quadrupole moments as probes of electronic and magnetic states of their parent atoms with the selectivity to the individual isotope of the element. Nuclear spins probe hyperfine fields produced by electronic spins and the nuclear quadrupole moments probe electric field gradients produced by an aspherical electron density distribution. Owing to this NMR is sensitive to the local environment. It allows us to probe internal fields brought about by the magnetic order and provides information on the magnetic and electronic state of an element at an individual structural and magnetic site. Performing the NMR experiments in an applied magnetic field can additionally provide information on the local arrangement of magnetic moments and the coupling between them.

The X-ray absorption spectroscopy in the range from about 10 eV below to 30 eV above the absorption edge, called X-ray absorption near edge structure (XANES), allows us to probe the valence state of an element and to obtain information on bonding, electron localisation, etc. Its "magnetic" counterpart, called X-MCD in the XANES range, allows us to investigate the magnetic properties of a system, and to determine separately the spin and orbital magnetic moments of an element. A combined analysis of the results of these two methods complemented with a conventional magnetic and structural characterisation will shed more light on the individual site electronic and magnetic properties of the compounds and their relation to the bulk properties.

2. Experimental

NMR measurements have been carried out with an automated, frequency swept spin-echo spectrometer [41]. The spin-echo spectra and the relaxation times have been measured at different temperatures (from 3 K to 300 K) and in applied magnetic fields on polycrystalline powder samples, the same as used in [12, 38].

The XAS (XANES) and X-MCD measurements on the Re $L_{2,3}$ edges have been carried out at Hasylab, DESY in Hamburg, at the station A1, which was particularly suited to XAS and X-MCD measurements. Experiments have been performed on polycrystalline powder samples at different temperatures (4.2 K, 10 K, and 300 K) and, for the X-MCD study, with applying a magnetic field up to 1 T. The measurements have been carried out in the transmission mode, in which the intensity of the incoming and transmitted monochromatic synchrotron light is measured and the absorption coefficient of the sample is determined as a function of energy.

The XAS (XANES) and X-MCD measurements on the Fe $L_{2,3}$ edges have been carried out at the ELETTRA Synchrotron Laboratory, Trieste, at the station BACH. Circularly polarized radiation was produced by a helical undulator ($P_{\mathrm{C}} > 99.5\%$) and monochromatised by spherical gratings. The spectra were recorded at room temperature for bulk polycrystalline samples of $\mathrm{AA}' = \mathrm{BaSr}$, Sr_2, and Ca_2 using total electron yield (TEY) detection technique. Four con-

secutive XAS measurements, two for each helicity, were performed on samples magnetised *ex situ* to 50 kOe and placed on a small Nd–Fe–B permanent magnet.

3. Molybdenum NMR results and discussion

In order to study the influence of A site substitution (i.e., the influence of changes in the crystallographic structure) on the local electronic and magnetic properties of Fe–Mo DP, ^{95}Mo and ^{97}Mo NMR measurements on several A_2FeMoO_6 compounds have been carried out [20, 42]. In all the cases, the observed main line is in the range of 50–80 MHz, and in the range of 30–60 MHz for low frequency satellites, Fig. 1, which are attributed to the ideal and defect sites of Mo ions, respectively [43, 20, 44]. For Ba_2FeMoO_6 the signal observed at 63.1(2) MHz is attributed to ^{57}Fe as derived from the measurements in the applied field which are discussed below. The Fe signals have recently been reported by Wojcik [45] although no proper identification of the gyromagnetic ratio through the measurements in the applied field was given.

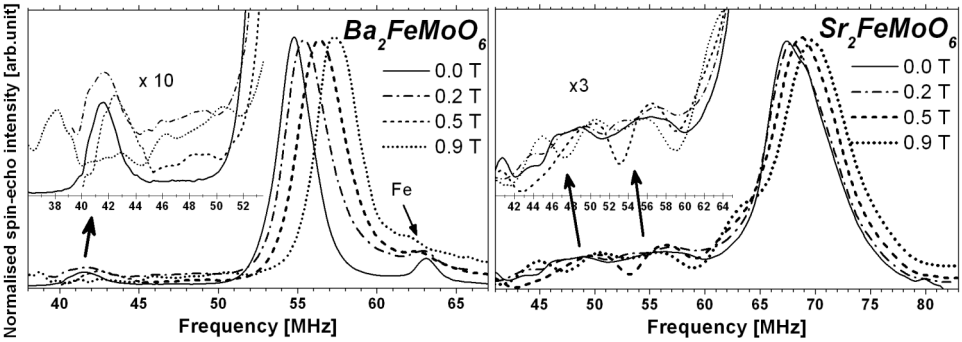

Fig. 1. The Mo and Fe NMR spin-echo spectra of Ba_2FeMoO_6 and Sr_2FeMoO_6, at 4.2 K and at the applied magnetic field.

From the central frequencies of the main lines, the values of the Mo hyperfine field (HF) are obtained and the corresponding values of the Mo magnetic moment are derived using the hyperfine coupling constant after [46]. The maximum value of HF and T_C are obtained for $A_2 = Sr_2$, which corresponds to the ideal crystallographic structure ($f \approx 1$). Decreasing the crystallographic symmetry with substitution $A_2 = Ba_2$, BaSr, and Ca_2, with $f \neq 1$, causes the decrease in Mo HF (and the related 4*d* electron population and magnetic moment) and T_C. Within the theoretical model of Sarma [26], where the Mo 4*d* exchange splitting is attributed to the Fe–Mo interaction, the above mentioned HF dependence on f suggests that the Fe–Mo interaction strength depends non-monotonously on the structural factor, being maximum for $f \approx 1$. Thus, the results indicate that the strongest enhancement of the Mo 4*d* splitting occurs for Sr_2FeMoO_6 where the highest Mo magnetic moment and the highest T_C values are observed [47, 20, 12].

The analysis of the ^{57}Fe resonance using the gyromagnetic ratio $\gamma_{\mathrm{Fe}} = 1.38$ MHz/T gives the HF value of 45.7(2) T, which is in good agreement with the Mössbauer results [18]. The much smaller intensity of the Fe signal is caused by the fact that the product of the natural isotopic abundance and the relative sensitivity for equal number of nuclei, which amounts 7.38×10^{-5} for ^{57}Fe, which is much smaller than those for the Mo isotopes which amount to 50.78×10^{-3} and 32.45×10^{-3}, for ^{95}Mo and ^{97}Mo, respectively.

The magnetisation curves at $T = 6$ K of the A_2FeMoO_6 (A_2 = Ba_2, SrBa, Sr_2, and Ca_2) compounds are presented in Fig. 2 together with the data normalised to the saturation magnetisation. As it can be seen, the theoretical saturation magnetisation value of 4 μ_{B}/f.u. for both possible localised valence states models: Fe^{3+}/Mo^{5+} or Fe^{2+}/Mo^{6+} as well as for the delocalised model is not attained. The existence of defect sites in the sample would explain why the theoretical value of the magnetisation is not reached. A comparison of these data and the corresponding NMR spectra shows that the larger the amount of defects in the sample is the lower the magnetisation is observed [48, 12, 8].

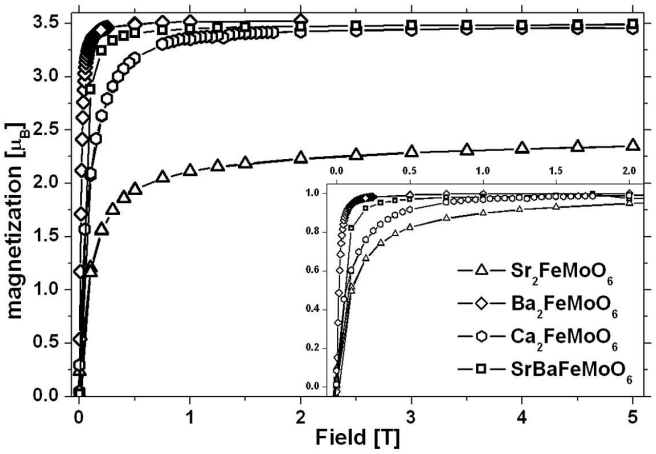

Fig. 2. Magnetisation curves of the AA′FeMoO$_6$ series at 6 K. In the inset the magnetisation data normalised to their values of the saturation magnetisation are presented.

In order to distinguish between the two types of defects (antisite ions and antiphase boundaries), NMR experiments under applied magnetic field (up to 0.9 T) on Ba_2FeMoO_6 and Sr_2FeMoO_6 compounds have been carried out. The results are presented in Fig. 1. For Ba_2FeMoO_6 there exists a single low frequency peak at 41.6 ± 1.7 MHz. No significant change of its resonant frequency between 0 T and 0.2 T can be attributed to the demagnetisation effect. This resonance line shifts towards higher frequencies with the applied field of 0.5 T. Between 0.5 T and 0.9 T its resonance frequency undergoes a step-like decrease from 42.7±1.2 MHz to 38.0±1.5 MHz. For Sr_2FeMoO_6 two structured low frequency peaks are observed at

57.1 MHz and 48.5 MHz, at zero field. No significant changes of the line positions are observed between 0 T and 0.2 T, due to the demagnetisation effect, as in Ba_2FeMoO_6. The lower frequency resonance line shifts towards higher frequencies for 0.5 T and splits at 0.9 T into two lines centred at 50.2 MHz and 44.9 MHz. The upper resonance line shifts towards lower frequencies as the applied field increases.

The shift of the low frequency satellite line of the Ba_2FeMoO_6 spectrum and the lowest satellite of the Sr_2FeMoO_6 spectrum toward higher frequencies with the applied magnetic field indicates that their Mo HF is parallel to the applied field, similarly to that of the main line. So that the corresponding Mo magnetic moments are antiparallel to the Fe moments. The values of the hyperfine fields of these satellite lines are lower from those of the respective main lines by approximately 1/5 to 1/4 of their values. Thus these resonances can be attributed to the Mo ions neighbouring a Mo AS. For such ions a reduction of the probability of the double exchange (DE)-like electron hopping to-and-from adjacent Fe ions by approximately 1/6 is expected as compared to that of the DE-like electron hopping between ideal sites. Consequently, a reduction of the $4d$ electron density and the respective Fermi contact term in the HF by approximately 1/6 can be deduced. As the other contributions to the effective field at the nucleus can also be present, the agreement between the above evaluated reduction of HF at the Mo AS neighbour by 1/6 and the experimentally obtained 1/4 and 1/5 can be regarded as satisfactory.

The amount of Mo AS defects deduced from the 1/6 of the intensity (area) of the corresponding lowermost satellite line is of 2.1%, 2.2%, 3.3% and 1% for the A_2FeMoO_6 compounds, where $A_2 = Ca_2$, Sr_2, SrBa, and Ba_2, respectively. As the strength of the magnetic coupling between two neighbouring Mo magnetic moments is estimated to be very weak [10, 29], a flip of the electron spin of the Mo AS ion is expected to occur at a relatively small applied magnetic field. This should be reflected in the change of the resonant frequency with the applied field, which is indeed observed for the Ba_2FeMoO_6 satellite line and an indication of this effect can also be seen for the lower frequency satellite in the Sr_2FeMoO_6 spectrum.

The shift towards lower frequencies with the applied magnetic field observed for the upper low frequency satellite of Sr_2FeMoO_6, opposite to the shift of the main line, suggests that this signal comes from Mo ions with their magnetic moments parallel to the applied magnetic field. This situation can be expected for Mo ions adjacent to Fe AP boundaries in the antiparallel (minority) domain. The applied magnetic field of 1 T is too weak to align the magnetic moments of both domains in parallel. The observed additional split of the lower satellite into two lines together with the decrease in the resonant frequency of the upper satellite line can be attributed to the presence of Fe AP domains, which couple antiparallel due to the antiferromagnetic coupling of adjacent Fe spins. Thus the directions of Mo HF corresponding to the observed NMR line in both antiparallel domains are

antiparallel and shift in opposite directions in the applied field. The satellite at the low frequency side of the main line at 0.9 T, shifting towards lower frequencies with the applied magnetic field can be attributed to the ideal Mo sites in the minority AP domains, where the Mo moments align parallel to the applied field (Fe moments in the minority AP domains are antiparallel to the applied field). The satellite line has too large intensity and too large change of frequency with the field to be attributed to the ^{57}Fe resonance.

The existence of a considerable amount of AP defects in Sr_2FeMoO_6 is in agreement with the magnetisation data, Fig. 2. The observed decrease in the bulk magnetisation, as well as the magnetic field much larger than 5 T needed for the magnetic saturation is mainly caused by the existence of the Fe AP boundaries. In the case of AS defects, the decrease in the magnetisation is proportional to the number of AS ions, whereas in the case of AP boundaries it is proportional to the volume of minority Fe AP domains. Resonance lines corresponding to antisite Mo ions, Mo ions in the AP boundaries and Mo ions close to more than one Mo AS can also be expected to appear in the NMR spectra. However, these NMR signals would have to appear at low frequencies and to exhibit a large quadrupolar interaction and, consequently, a fast relaxation, which prevents their observation.

The ^{57}Fe NMR resonance is observed for Ba_2FeMoO_6 as a weak resolved signal of the spin echo shape different from that of molybdenum. It shifts towards lower frequencies with the applied magnetic field and the slope of the field dependence of its resonant frequency amounts to –1.4(2) MHz/T. This is in good agreement with the value of the ^{57}Fe gyromagnetic ratio, 1.38 MHz/T. The shift of the Fe line with a full gyromagnetic ratio suggests that the Fe magnetic moment (the Fe HF) is parallel (antiparallel) to the applied magnetic field.

For Ba_2FeMoO_6 a small peak at 78.5(3) MHz is also observed. This peak can be attributed to Fe^{3+}, in agreement with Yokoyama [43] and corresponds to a HF equal to 56.9(2) T. The presence of some Fe^{3+} in these compounds is confirmed by the Mössbauer experiments [18, 49, 50] and by XAS measurements presented in the next Section. The lack of a possible signal of the charge localised Mo^{5+} can be explained by its smearing out due to a large spin–dipole and, possibly, orbital hyperfine field. A quadrupole splitting and quadrupole relaxation related to the fact that the $4d$ electron would be localised at the spin down t_{2g} orbital could also prevent the observation of the Mo^{5+} signal. The electrons delocalised over adjacent Mo and Fe sites, on the contrary, undergo fast hopping between different t_{2g} orbitals of a Mo ion, which results in averaging the quadrupole splitting as well as the spin–dipole and orbital contributions to the Mo HF and the signal is not affected by the splitting arising from these anisotropic contributions.

The ^{95}Mo and ^{97}Mo NMR spin-echo spectra for $SrBaFeMoO_6$, at various temperatures are presented in Fig. 3. The main line corresponding to the ideal Mo sites and the low frequency satellites corresponding to the defect sites are observed in all the spectra. The NMR resonance frequencies for both lines shift

toward lower frequencies when the temperature increases. The central frequencies of the main line and of the satellite lines have been derived from the spectra at each temperature. Figure 4 presents the central frequencies and the magnetisation data normalised to their values at 4.2 K, for a comparison. The dashed lines show the fits of the temperature dependence of the Mo resonant frequency ν, which represents HF related to the mean value of the z-th component of the Mo spin, $\langle S_z \rangle$ [51, 20]. Considering the $T^{3/2}$ and $T^{5/2}$ terms of a Bloch temperature dependence [52], a better fit of ν (twice smaller χ^2) is obtained for the $T^{5/2}$ dependence: $\nu(T) = \nu(4.2\text{ K}) \times (1 - bT^{5/2})$. This indicates that the investigated Fe–Mo double perovskites are half-metals [53]. A fit of the function $\nu(T) = \nu(4.2\text{ K}) \left(1 - aT^{3/2} - bT^{5/2}\right)$ for $SrBaFeMoO_6$ provides the a/b ratio of 170 K, whereas the theoretical calculation assuming Heisenberg-model ferromagnets with cubic symmetry, the a/b ratio is greater than 1400 K, after [52]. This result shows that the dominacy of the $T^{5/2}$ term in the Fe–Mo DP can be attributed to their half-metallic character.

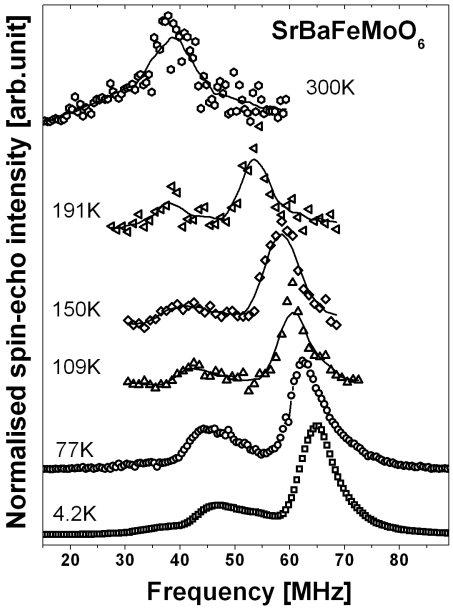

Fig. 3. The Mo NMR spin-echo spectra of $SrBaFeMoO_6$ at different temperatures. The maximum intensity in each spectrum is normalised to unity. The line is a guide for the eye.

The NMR spectra of the A_2FeReO_6 compounds consist of signals of ^{185}Re and ^{187}Re isotopes, which are unresolved due to very similar values of their gyromagnetic ratios [20]. The values of the hyperfine fields derived from the resonance frequencies amount to 84 T, 94 T and 95 T for Ba, Sr and Ca compounds, respectively. The hyperfine coupling constant of –100 T/μ_B was used [46]. The values of

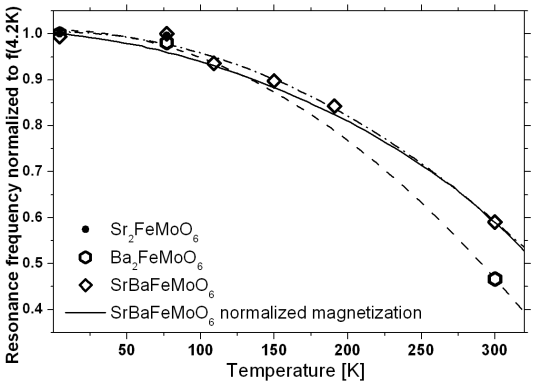

Fig. 4. Temperature dependence of hyperfine fields of the main lines of the $AA'FeMoO_6$ compounds (ideal Mo sites) normalised to their values at 4.2 K. Dashed lines are the fitted $T^{5/2}$ dependence and the solid line is the normalised magnetisation for $SrBaFeMoO_6$.

Re magnetic moments derived from hyperfine fields amount to –0.87 μ_B, –0.94 μ_B, and –0.95 μ_B for the Ba, Sr, and Ca compounds, respectively. In analogy with the Mo moments they are assumed to be antiparallel to the Fe moments, which is confirmed by X-MCD measurements.

A plot of the main resonant frequencies and the corresponding values of magnetic moments in A_2FeMoO_6 and A_2FeReO_6 compounds are shown in Fig. 5, together with theoretical values of the magnetic moments obtained from Ref. [29]. For the case of the Mo compounds, there is a very good agreement between the experimental and theoretical results. However, the experimental data for Re compounds are lower than theoretically predicted, which is attributed to the presence of orbital contribution to the Re magnetic moment [54].

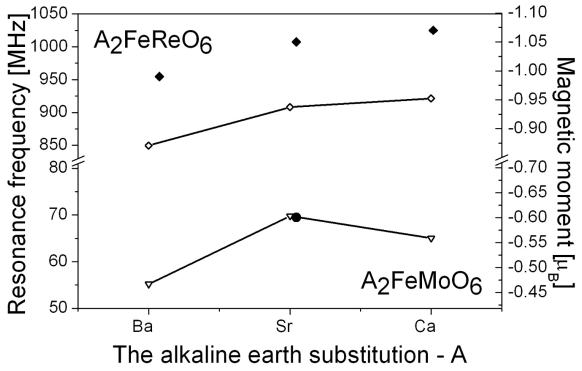

Fig. 5. Resonance frequencies (left axis) and magnetic moments at M = Mo or M = Re (right axis) of $AA'FeMO_6$ for different alkaline earth compounds. Open triangles and rhombuses represent experimental data. Filled circle and rhombuses correspond to theoretical values of magnetic moments from Ref. [6].

4. XANES results and discussion

The spectra at the Mo K edge of the $AA'FeMoO_6$ ($AA' = Sr_2$, SrBa, and Ba_2) compounds are presented in Fig. 6. For a better visualisation of the characteristic features of the XANES spectra, their first derivatives are also shown in the figure. The maxima in the first derivative reflect the largest slope of the DOS function. For all the compounds studied, three peaks, marked in Fig. 6, can be distinguished in the spectra: A — a pre-peak, B — first main peak, and C — second main peak. The pre-peak A is attributed to the $1s \rightarrow 4d$ transitions, either quadrupole allowed or dipole forbidden for an octahedral environment. It is clearly visible for Ba_2FeMoO_6. This transition is allowed due to the hybridisation of O $2p$ and Mo $4d$ states. The first and the second main peaks, B and C, are attributed to the excitations of $1s$ electrons to the empty $5p$ states [55, 56].

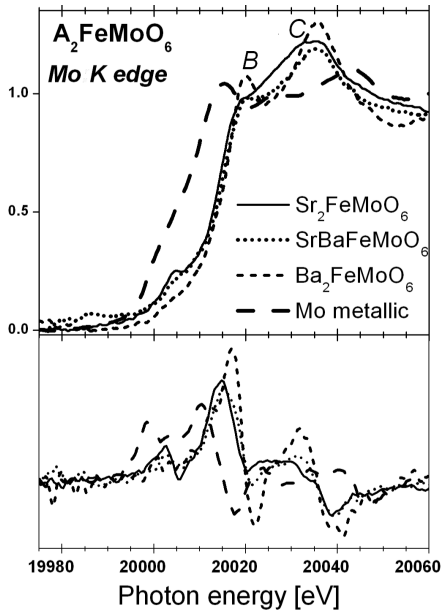

Fig. 6. The normalised Mo K-edge XANES spectra (top) with their first derivatives (bottom) for the $AA'FeMoO_6$ ($AA' = Sr_2$, SrBa, and Ba_2) compounds.

The energy corresponding to the half height of the edge step, which is a measure of the Fermi energy, has been determined. Its increase is observed along the Sr_2FeMoO_6, $SrBaFeMoO_6$ and Ba_2FeMoO_6 series, Fig. 8. The effect has been related to the increase in the tolerance factor from $f = 1.007$ (Sr_2FeMoO_6) to 1.07 (Ba_2FeMoO_6), which is found to correspond to a decrease in the Mo $4d$ electron occupation and the related Mo magnetic moment. The values of the edge energies reveal that the molybdenum valence state is between 5+ and 6+, for all the compounds. This is in agreement with the results presented in [56].

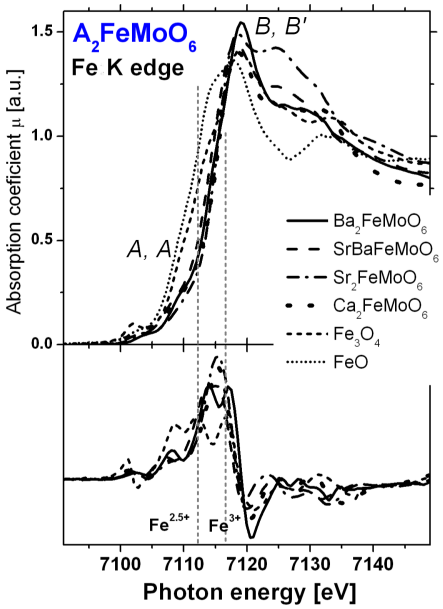

Fig. 7. The normalised Fe K-edge XANES spectra (top) with their first derivatives (bottom) for the AA′FeMoO$_6$ (AA′ = Ca$_2$, Sr$_2$, SrBa, and Ba$_2$) compounds. Energies corresponding to $Fe^{2.5+}$ and Fe^{3+} features in the Fe_3O_4 spectrum are marked with grey dashed lines.

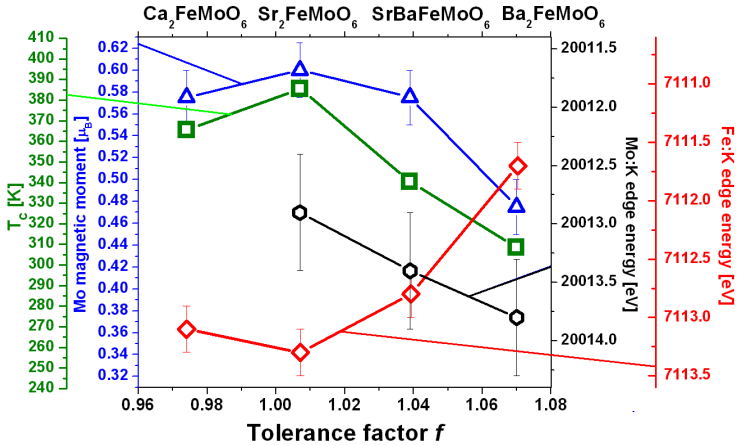

Fig. 8. The Mo magnetic moment (triangles), T_C (squares), and the Fe K (rhombuses) and Mo K (hexagons) edge energies vs. tolerance factor f, for AA′FeMoO$_6$ double perovskites (AA′ = Ca$_2$, Sr$_2$, SrBa, Ba$_2$).

The difference of the edge energies of MoO_3 (Mo^{6+}) and $SrMoO_3$ (Mo^{4+}), which amounts to 3.2 eV, provides the approximate value of chemical shift at the Mo K

edge of 1.6 eV per unit of the valence [56]. The corresponding difference of the $4d$ electron occupation derived from the edge energies of Ba_2FeMoO_6 and Sr_2FeMoO_6 in this work (0.9 eV) would amount to 0.6(3) of an electron.

In addition to the edge energy shift a narrowing of both B and C main peaks, a smearing out of the pre-peak A and a shift of the peak C toward higher energies is observed with the alkaline earth substitution (see Fig. 6). The narrowing of the peaks B and C indicates that the density of empty $5p$ states above the Fermi level becomes narrower with the increase in the tolerance factor from $f = 1.007$ (Sr_2FeMoO_6) to 1.07 (Ba_2FeMoO_6).

The measurements on the Fe K edge have been performed on the $AA'FeMoO_6$ ($AA' = Ca_2$, Sr_2, SrBa, and Ba_2) compounds. The spectra with their first derivatives are shown in Fig. 7. The variation of the energy of the half height of the edge step along the series, which is a measure of the Fermi energy, has been illustrated in Fig. 8. In Fig. 7 the characteristic peaks are marked as A, A', B, and C. Features A and A', which represent "pre-peaks", appear in the energy range of 7100–7115 eV. The white line, i.e. the main peak appearing directly above the absorption edge, at about 7120 eV, is marked as B, and a weaker, broad maximum at the energies of 7125–7130 eV is marked as C. These maxima correspond to the excitations of $1s$ electrons to the empty $4p$ states above the Fermi level. The results, in agreement with recent results on Fe K edge [56], are similar to those observed for the Mn K edge in $LaMnO_3$ [57, 58] and obtained in theoretical calculations [25, 27, 59, 28, 29, 60, 30]. The origin of pre-peaks (features A and A') is related to the transition of $1s$ electrons to $3d$ states (the quadrupole transition for an octahedral environment) [61]. This transition is possible only if the overlap of the Fe $3d$ states and O $2p$ states provides a hybridisation of the $4p$ and $3d$ states of iron.

The pre-peaks $A-A'$ exhibit some changes of their positions and magnitude with the A site ion substitution. The previous studies of Fe–Mo DP using the photoemission spectroscopy (PES) show that the distance between occupied Fe $3d$ e_g and t_{2g} spin up states is about 2 eV and the distance between Fe $3d$ states and O $2p$ states is about 5 eV [26, 59, 62, 32, 34]. Thus, the pre-peak A in the Fe XANES spectra can be attributed to the $4p$ states hybridised with oxygen $2p$ states and iron t_{2g} spin up states, whereas the pre-peak A$'$ can be assigned to the $4p$ states hybridised with iron e_g spin up and t_{2g} spin down states. The separation of the peaks A–A$'$ varies from 6.1(2) eV for Sr_2FeMoO_6 to 5.0(2) eV for Ca_2FeMoO_6 and 5.4(2) eV for Ba_2FeMoO_6. The value of the splitting is the smallest for the largest deviation of the structural tolerance factor f from unity.

Significant changes of the shape of the spectra, Fig. 7, can be attributed mainly to the variation of the tolerance factor, similarly to those occurring in the Mo K edge spectra of the series. It is worth noting that the most pronounced white line peak in the Fe K edge spectrum of Ba_2FeMoO_6 corresponds to the least pronounced white line in its Mo K edge spectrum. Analogously, the least

pronounced white line in the Fe K edge spectrum of Sr_2FeMoO_6 corresponds to the least pronounced white line in its Mo K edge spectrum. A more pronounced white line corresponding to the empty final state (Mo $5p$ and Fe $4p$) can be related to a narrowing of the DOS with increasing intra-ionic distances (and the tolerance factor f) along the series.

A careful analysis of the main edge structure, Fig. 7, lower part, shows that the first derivative of the XANES spectrum exhibits two peaks for Ba_2FeMoO_6 and one peak for Ca_2FeMoO_6 and Sr_2FeMoO_6. This means that the main edge consists of two steps for Ba_2FeMoO_6, whereas for Ca_2FeMoO_6 and Sr_2FeMoO_6 a single step occurs. A flat peak in the first derivative of $SrBaFeMoO_6$ indicates the presence of two steps close one to another. The appearance of a two-step edge is similar to that of the XANES spectrum at the Fe K edge of magnetite, Fe_3O_4, at 300 K (see Fig. 7) and to the results presented in [56]. The two steps have been attributed to the two distinct iron valence states $Fe^{2.5+}$ (lower step) and Fe^{3+} (upper step) [63, 64]. The two maxima in the first derivative of the XANES spectrum of Ba_2FeMoO_6 coincide with the respective maxima in the XANES spectrum of Fe_3O_4, and therefore they have tentatively been attributed to the ionic state Fe^{3+} (upper) and to the intermediate, "metallic" state between Fe^{3+} and Fe^{2+} (lower), close to $Fe^{2.5+}$.

The maxima in the first derivative of the XANES spectra for Ca_2FeMoO_6 and Sr_2FeMoO_6 appear at the energies between the two maxima for Ba_2FeMoO_6, which indicates an intermediate, "metallic" valence state between $Fe^{2.5+}$ and Fe^{3+} in these compounds. A two-step character can also be found in the Mo K edge XANES spectrum, Fig. 6. The smaller maximum of the first derivative at the lower energy side of the main maximum can possibly be attributed to the presence of the Mo^{5+} states, which would be the local counterparts of the Fe^{3+} states at the XAS timescale, i.e. 10^{-15} s.

A close similarity between the dependence of the Mo magnetic moment and T_C on the tolerance factor, Fig. 8, indicates that the strength of the magnetic interaction between Fe and Mo is related to the magnetic moment and the corresponding $4d$ electron occupation at the molybdenum site. A higher T_C is observed for a larger value of the magnetic moment (larger electron density) at Mo. This result is consistent with the prediction of the theoretical model in which the increase in T_C is related to the increase in the Mo $4d$ splitting, determined by the strength of the exchange interaction between Mo and Fe [26]. Thus, the increase (decrease) in the Mo $4d$ splitting would lead to the increase (decrease) in the $4d$ electron population at the Mo site at the cost of the $3d$ electron population at the Fe site, as deduced from the opposite tendencies of the edge energies, Fig. 8. The largest Mo moment (and the largest $4d$ electron occupation) corresponding to the strongest electron transfer is observed for Sr_2FeMoO_6, where the tolerance factor f is the closest to unity. The departure of f from unity towards lower and higher values results in a decrease in the Mo moment and of T_C, which is related to a decrease in the Mo $4d$ exchange splitting.

The Re $L_{2,3}$ XANES spectra of the $AA'FeReO_6$ ($AA' = Ca_2$, SrCa, Sr_2, BaSr, and Ba_2) compounds presented in [54] have a similar shape, dominated by a very intense "white line" feature due to the transition into nearly empty final d states. The white line feature at the Re L_3 edge is asymmetric, with a tiny bulge at around 3 eV below its maximum, which can be attributed to the splitting of the t_{2g} and e_g final states [17]. We did not observe any difference in shape between the spectra of the compounds studied, which might be attributed to the lattice distortion. The only difference observed is a gradual decrease in the first moment of the Re $L_{2,3}$ edge spectra by 0.4 eV from ReO_3 to Ba_2FeReO_6 and further by 0.15 eV and 0.3 eV for Sr_2FeReO_6 and Ca_2FeReO_6, respectively. The latter result indicates that all the compounds studied reveal the effective valence state slightly lower than Re^{6+}, that decreases with introducing smaller A-site ions, which is in agreement with the Fe valence evolution observed by Mössbauer spectroscopy [65, 36, 66]. Nevertheless, due to a low accuracy of the method of analysis and strong covalent effects in these compounds, quantitative assignment of the formal valence would be unreliable.

5. X-MCD results and discussion

The Re $L_{2,3}$ edge X-MCD spectra of the $AA'FeReO_6$ ($AA' = Ca_2$, SrCa, Sr_2, BaSr, and Ba_2) compounds are presented in [54]. The L_3 edge signal shows differential-like shape with a minimum at the edge energy and a positive peak close to the maximum. The integrated X-MCD at Re L_3 edge is positive for all the compounds studied except for Ca_2FeReO_6. All the measured Re L_2 edge X-MCD spectra consist of a single broad negative peak, that is approximately eight times larger than the maximum of the L_3 edge spectra.

Recently, Jeng and Guo, in their theoretical study of magnetic moments in Sr_2FeReO_6 [30] found that the Re $5d$ orbital down-spin states are highly polarised in spite of the octahedral ligand field, leading to a large unquenched orbital moment. Moreover they observed strong tendency to occupy the $m = 1$ (t_{2g}) magnetic orbitals by Re electrons. Using the orbital occupation numbers given in Ref. [30] one can predict the relative intensity of the X-MCD spectra using oscillator strengths for electronic excitation [67]. According to such an analysis the integrated Re L_3 edge X-MCD spectra ought to be positive and ten times less intense than the negative L_2 edge spectra. Moreover, if Re $5d$ t_{2g} and e_g subbands are considerably splitted in energy, the L_3 edge X-MCD ought to show differential-like shape due to negative (positive) contribution from excitation to t_{2g} (e_g) orbital, whereas the L_2 edge ought to reveal a single broad peak due to negative contribution from both kinds of excitation.

The latter predictions are unambiguously confirmed by our experimental results [54]. The Re L_3 edge dichroic spectra show differential-like shape with a minimum at the edge energy and a positive peak close to the maximum. The integrated X-MCD at Re L_3 edge is positive for all the compounds studied except

for Ca_2FeReO_6. All the measured Re L_2 edge X-MCD spectra consist of a single broad negative peak, that is approximately eight times larger than the maximum of the L_3 edge spectra as expected for system with dominantly occupied $m = 1$ orbitals. The latter discovery proves that the orbital moment of the Re $5d$ electrons is not fully quenched. A careful analysis reveals that the main difference in shape of the spectra between compounds studied is due to a contribution from $5d$ t_{2g} subband, which is revealed in larger negative peks at the $L_{2,3}$ edges as well as in a shifted L_2 edge minimum to lower energy in Ca_2FeReO_6. This behaviour is attributed to increase in t_{2g} band polarisation due to rise in electronic occupation of spin-down t_{2g} subband with increase in lattice distortion.

In order to derive the values of orbital, spin, and total magnetic moment of rhenium from $L_{2,3}$ X-MCD spectra the sum rules [68, 69] method has been applied. According to this theory, the sum of integrated intensities of the X-MCD spectra at both $L_{2,3}$ edges is proportional to the orbital moment (m_L), whereas the difference of L_3 and doubled L_2 integral is proportional to the spin (m_S) moment and magnetic-dipole term, which can be neglected in the case of polycrystalline samples. In final relations the accurate values of moments are obtained by normalisation to the "white line" intensity and to the number of $5d$ holes (n_h) derived from XAS spectra and Mssbauer spectroscopy results [65, 36, 66]. The obtained spin and orbital moments of rhenium are antiparallel, as expected from the third

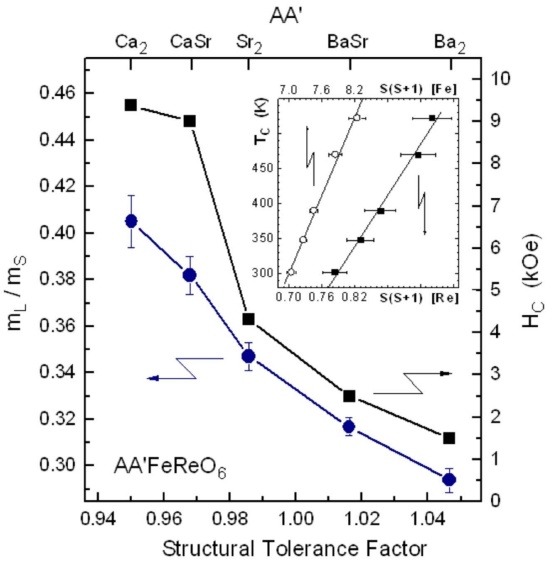

Fig. 9. Orbital moment of rhenium and coercive field of the compounds studied plotted versus structural tolerance factor. Both measurements were performed at $T = 10$ K. Inset shows the dependence of T_C versus effective spin moment of Fe (open circles) and Re (filled squares) ions.

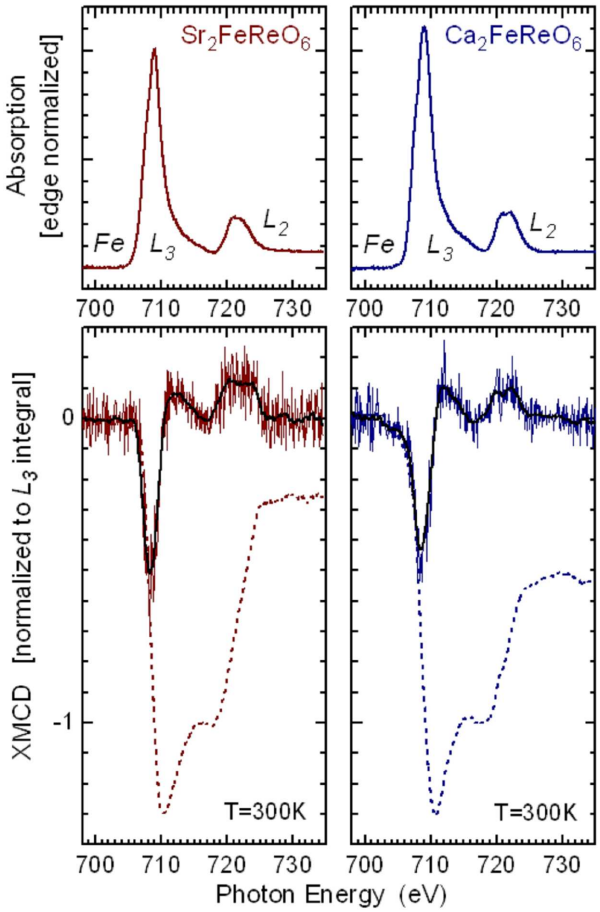

Fig. 10. X-ray absorption (upper parts) and X-MCD (lower parts) spectra of Sr_2FeReO_6 and Ca_2FeReO_6 at the $L_{2,3}$ edges of iron measured at room temperature. In the lower parts the thin and thick solid lines denote "as measured" and smoothed (over 1 eV) X-MCD spectra, respectively, whereas dotted lines represent integral of measured spectra.

Hund rule. The resulting total Re moment is antiferromagnetically coupled to the Fe moment and is estimated at $m_{\mathrm{tot}} \approx 0.8\ \mu_{\mathrm{B}}$, in good agreement with the recent NMR [20] and neutron diffraction results [37]. Moreover, the spin moment of order of 1.1 μ_{B} is consistent with the predictions of local spin density calculations [29, 31].

The total magnetic moment of Re in the $AA'FeReO_6$ series does not alter significantly within the series, similarly to bulk magnetisation [38], whereas the orbital moment shows a correlation with lattice distortion, Fig. 9. The spin and orbital contributions are both increasing with lattice distortion, indicating a

strengthening of magnetic interactions. In particular, the increase in orbital moment by 50% between Ba_2FeReO_3 and Ca_2FeReO_6 is an unambiguous indication of a strengthening of the spin–orbit coupling in distorted compounds, as suggested by De Teresa et al. [38]. A comparison of the local magnetic moment evolution to the macroscopic magnetic properties of the compounds studied reveals a correlation with the Curie temperature. An approximately linear dependence of T_C on the effective spin moment, $S(S+1)$, of iron and rhenium, inset of Fig. 9, is similar to that predicted for Heisenberg-like exchange interactions. From a comparison of the rhenium orbital moment with the evolution of other unique magnetic property of the compounds studied, the high coercive field, Fig. 10, the intriguing conclusion may be drawn. Although the values of both quantities increase with lattice distortion, the evolution of the orbital contribution is less steep comparing with that of the coercive field on moving to monoclinic compounds. Since the latter property is linked to the anisotropy of orbital moment [70], the additional contribution from the iron orbital moment can be expected. The results of the X-MCD measurements at Fe $L_{2,3}$ edges at room temperature are presented in Fig. 10. The spectra, normalised to the L_3 edge area, show a considerable difference of their integrals over both edges, which is a direct indication of difference in orbital to spin moment ratio. Derivation of m_L/m_S ratios provided their values of 0.02(3), 0.07(4) and 0.18(6) in AA′ = BaSr, Sr_2, and Ca_2, respectively. The latter results suggest the existence of a small positive orbital moment of Fe, which is consistent with more than half-filled Fe $3d$ band. A considerably larger Fe orbital moment in Ca_2FeReO_6 suggests that the orbital anisotropy of Fe $3d$ electrons may be an additional source of the large magnetocrystalline anisotropy observed in the monoclinic ordered Fe–Re double perovskites.

6. Conclusions

The results of a combined NMR, XAS and X-MCD study of the $AA'FeMoO_6$ and $AA'FeReO_6$ double perovskites presented in this work have led to the following findings:

— Mo bears a noninteger magnetic moment having its origin in the $4d$ spin-down electron density. The moment is antiparallel to that of iron and its value depends on the alkaline earth substitution. It is maximal for the compound with the structural tolerance factor of 1.

— The variation of the tolerance factor caused by the alkaline earth substitution leads to the d electron density transfer between the Fe and Mo sites whose rate depends on f. The highest $4d$ electron occupation at the Mo site is found for the compound with f closest to 1 and it decreases with the departure of f from unity.

— A higher $4d$ electron occupation at the Mo site results in a higher strength of the exchange interaction and, therefore, in a higher magnetic ordering temperature of the compound.

— Antisite atoms and antiphase boundaries are identified in NMR measurements. A flip of the Mo antisite ion moment is observed when the applied magnetic field is greater than 0.5 T, due to its weak exchange coupling with the neighbouring Mo ions. The magnetic field needed for the magnetic saturation of Sr_2FeMoO_6 is much higher than in the case of Ba_2FeMoO_6. This is attributed to the presence of antiphase boundaries in the former compound, which create magnetic pseudo-domains (minority domains) with opposite magnetisations.

— The dominant $T^{5/2}$ term in the temperature dependence of the Mo $\langle S_z \rangle$ and of the bulk magnetisation in the $AA'FeMoO_6$ compounds confirms the half metallic character of the compounds.

— The X-MCD study confirmed theoretical predictions that rhenium orbital moment is not quenched by octahedral ligand field in $AA'FeReO_6$ double perovskites. The magnetic moment of Re is of order of 0.8 μ_B and is antiparallel to that of Fe, which agrees with bulk magnetisation and NMR results. The effective total angular momentum of rhenium does not change significantly within the series, whereas the magnitude of the orbital contribution increases with the lowering of local symmetry of the compounds. An additional contribution from the Fe orbital moment in distorted compounds is revealed by Fe $L_{2,3}$ edges X-MCD study.

Acknowledgements

Synchrotron measurements were supported by the European Community under project HPRI-CT-1999-00033 and within the Research Infrastructure Action under the FP6 "Structuring the European Research Area" Programme (through the Integrated Infrastructure Initiative "Integrating Activity on Synchrotron and Free Electron Laser Science").

References

[1] D. Serrate, J.M. De Teresa, M.R. Ibarra, *J. Phys., Condens. Matter* **19**, 23201 (2005).

[2] F.S. Galasso, F.C. Douglas, R.J. Kasper, *J. Chem. Phys.* **44**, 1672 (1966).

[3] N. Auth, G. Jakob, W. Westerburg, C. Ritter, I. Bonn, C. Felser, W. Tremel, *J. Magn. Magn. Mater.* **272-276**, e607 (2004).

[4] C. Ritter, J. Blasco, J.M. De Teresa, D. Serrate, L. Morellón, J. García, M.R. Ibarra, *Solid State Sci.* **6**, 419 (2004).

[5] C. Ritter, J. Blasco, L. Morellon, J.M. De Teresa, J. Garcia, M.R. Ibarra, *J. Magn. Magn. Mater.* **226-230**, 1070 (2001).

[6] J. Blasco, C. Ritter, L. Morellon, P.A. Algarabel, J.M. De Teresa, D. Serrate, J. Garcia, M.R. Ibarra, *Solid State Sci.* **4**, 651 (2002).

[7] Y. Moritomo, Sh. Xu, A. Machida, T. Akimoto, E. Nishibori, M Takata, M. Sakata, *Phys. Rev. B* **61**, R7827 (2000).

[8] R.P. Borges, R.M. Thomas, C. Cullinan, R. Suryanarayanan, L. Ben-Dor, L. Pinsard-Gaudart, A. Revcolevschi, *J. Phys. Condens. Matter* **11**, L445 (1999).

[9] J. Navarro, C. Frontera, Ll. Balcells, B. Martinez, J. Fontcuberta, *Phys. Rev. B* **64**, 092411 (2001).

[10] A.S. Ogale, S.B. Ogale, R. Ramesh, T. Venkatesan, *Appl. Phys. Lett.* **75**, 537 (1999).

[11] J. Navarro, Ll. Balcells, F. Sandiumenge, M. Bibes, A. Roig, B. Martinez, J. Fontcuberta, *J. Phys. Condens. Matter* **13**, 8481 (2001).

[12] C. Ritter, M.R. Ibarra, L. Morellon, J. Blasco, J. Garcia, J.M. De Teresa, *J. Phys., Condens. Matter.* **12**, 8295 (2000).

[13] R.D. Shannon, C.T. Prewitt, *Acta Crystal. B* **25**, 925 (1969).

[14] V. Goldschmidt, *Geochemistry*, Oxford University Press, Oxford 1958.

[15] J.B. Philipp, P. Majewski, L. Alff, A. Erb, R. Gross, T. Graf, M.S. Brandt, J. Simon, T. Walther, W. Mader, D. Topwal, D.D. Sarma, *Phys. Rev. B* **68**, 144431 (2003).

[16] Y. Tokura, Y. Tomioka, *J. Magn. Magn. Mater.* **200**, 1 (1999).

[17] G. Popov, M. Greenblatt, M. Croft, *Phys. Rev. B* **67**, 24406 (2003).

[18] J.M. Greneche, M. Venkatesan, R. Suryanarayanan, J.M.D. Coey, *Phys. Rev. B* **63**, 174403 (2001).

[19] D. Serrate, J.M. De Teresa, J. Blasco, M.R. Ibarra, L. Morellon, C. Ritter, *Europ. Phys. J. B* **39**, 35 (2004).

[20] Cz. Kapusta, D. Zajac, P.C. Riedi, M. Sikora, C.J. Oates, J. Blasco, M.R. Ibarra, *J. Magn. Magn. Mater.* **272-276**, e1619 (2004).

[21] D. Zajac, Cz. Kapusta, P.C. Riedi, M. Sikora, C.J. Oates, D. Rybicki, J.M. De Teresa, D. Serrate, C. Marquina, M.R. Ibarra, *Acta Phys. Pol. A* **106**, 759 (2004).

[22] P.G. Radaelli, G. Iannone, M. Marezio, H.Y. Hwang, S.W. Cheong, J.D. Jorgensen, D.N. Argyriou, *Phys. Rev. B* **56**, 8265 (1997).

[23] M. Medarde, J. Mesot, P. Lacorre, S. Rosenkranz, P. Fisher, K. Gobrecht, *Phys. Rev. B* **52**, 9248 (1995).

[24] D. Serrate, J.M. De Teresa, J. Blasco, M.R. Ibarra, L. Morellon, C. Ritter, *Appl. Phys. Lett.* **80**, 4573 (2002).

[25] K.-I. Kobayashi, T. Kimura, H. Sawada, K. Terakura, Y. Tokura, *Nature* **395**, 677 (1998).

[26] D.D. Sarma, P. Mahadevan, T. Saha-Dasgupta, S. Ray, A. Kumar, *Phys. Rev. Lett.* **85**, 2549 (2000).

[27] Y. Tomioka, T. Okuda, Y. Okimoto, R. Kumai, K.Y. Kobayashi, Y. Tokura, *Phys. Rev. B* **61**, 422 (2000).

[28] Z. Fang, K. Terakura, J. Kanamori, *Phys. Rev. B* **63**, 180407(R) (2001).

[29] H. Wu, *Phys. Rev. B* **64**, 125126 (2001).

[30] H.-T. Jeng, G.Y. Guo, *Phys. Rev. B* **67**, 094438 (2003).

[31] Z. Szotek, W.M. Temmerman, A. Svane, L. Petit, H. Winter, *Phys. Rev. B* **68**, 104411 (2003).

[32] J.-S. Kang, S.C. Wi, S.S. Lee, G. Kim, H.M. Yang, B.W. Lee, S.W. Han, K.H. Kim, A. Sekiyama, S. Kasai, S. Suga, J.H. Shim, B.I. Min, *J. Phys., Condens. Matter* **16**, S5685 (2004).

[33] J. Fontcuberta, D. Rubi, C. Frontera, J.L. Garcia-Munoz, M. Wojcik, E. Jedryka, S. Nadolski, M. Izquierdo, J. Avila, M.C. Asensio, *J. Magn. Magn. Mater.* **290-291**, 974 (2005).

[34] T. Saitoh, M. Nakatake, H. Nakajima, O. Morimoto, A. Kakizaki, Sh. Xu, Y. Moritomo, N. Hamada, Y. Aiura, *J. Electron Spectrosc. Relat. Phenom.* **144-147**, 601 (2005).

[35] H. Kato, T. Okuda, Y. Okimoto, Y. Tomioka, K. Oikawa, T. Kamiyama, Y. Tokura, *Phys. Rev. B* **65**, 144404 (2002); H. Kato, T. Okuda, Y. Okimoto, Y. Tomioka, Y. Takenoya, A. Ohkubo, M. Kawasaki, Y. Tokura, *Appl. Phys. Lett.* **81**, 328 (2002).

[36] T. Alamelu, U.V. Varadaraju, M. Venkatesan, A.P. Douvalis, J.M.D. Coey, *J. Appl. Phys.* **91**, 8909 (2002).

[37] W. Westerburg, O. Lang, C. Ritter, C. Felser, W. Tremel, G. Jakob, *Solid State Commun.* **122**, 201 (2002).

[38] J.M. De Teresa, D. Serrate, J. Blasco, M. R. Ibarra, L. Morellon, *Phys. Rev. B* **69**, 144401 (2004).

[39] H. Kato, T. Okuda, Y. Okimoto, Y. Tomioka, K. Oikawa, T. Karniyama, Y. Tokura, *Phys. Rev. B* **69**, 184412 (2004).

[40] D. Serrate, J.M. De Teresa, J. Blasco, L. Morellon, M.R. Ibarra, *J. Magn. Magn. Mater.* **290-291**, 1021 (2005).

[41] J.S. Lord, P.C. Riedi, *Measur. Sci. Technol.* **6**, 149 (1995).

[42] D. Zajac, Cz. Kapusta, P.C. Riedi, M. Sikora, C.J. Oates, D. Rybicki, J. Blasco, D. Serrate, J.M. De Teresa, M.R. Ibarra, *J. Magn. Magn. Mater.* **272-276**, 1756 (2004).

[43] H. Yokoyama, T. Nakagawa, *J. Phys. Soc. Japan* **28**, 1197 (1970).

[44] M. Wojcik, E. Jedryka, S. Nadolski, J. Navarro, D. Rubi, J. Fontcuberta, *Phys. Rev. B* **69**, 100407 (2004).

[45] M. Wojcik, E. Jedryka, S. Nadolski, D. Rubi, C. Frontera, J. Fontcuberta, B. Jurca, N. Dragoe, P. Berthet, *Phys. Rev. B* **71**, 104410 (2005).

[46] I.A. Campbell, *J. Phys. C, Solid State Phys.* **2**, 1338 (1969).

[47] Cz. Kapusta, P.C. Riedi, D. Zajac, M. Sikora, J.M. De Teresa, L. Morellon, M.R. Ibarra, *J. Magn.Magn. Mater.* **242-245**, 701 (2002).

[48] D. Sanchez, M. Garcia-Hernandez, J.L. Martinez, J.A. Alonso, M.J. Martinez--Lope, M.T. Casais, A. Mellergard, *J. Magn. Magn. Mater.* **242-245**, 729 (2002).

[49] J. Linden, M. Karppinen, T. Shimada, Y. Yasukawa, H. Yamauchi, *Phys. Rev. B* **68**, 174415 (2003).

[50] J. Żukrowski, Cz. Kapusta, D. Zając, unpublished data.

[51] D.A. Shirley, S.S. Rosenblum, E. Matthias, *Phys. Rev.* **170**, 363 (1968).

[52] F.J. Dyson, *Phys. Rev.* **102**, 1230 (1956).

[53] A.Z. Solontsov, *J. Magn. Magn. Mater.* **140-144**, 215 (1995).

[54] M. Sikora, Cz. Kapusta, M. Borowiec, C.J. Oates, V. Procházka, D. Rybicki, D. Zajac, J.M. De Teresa, C. Marquina, M.R. Ibarra, *Appl. Phys. Lett.* **89**, 62509 (2006).

[55] F. Rocca, A. Kuzmin, P. Mustarelli, C. Tomasi, A. Magistris, *Solid State Ionics* **121**, 189 (1999).

[56] J. Herrero-Martin, J. Garcia, G. Subias, J. Blasco, M.C. Sanchez, *J. Phys., Condens. Matter* **16**, 6877 (2004).

[57] M. Benfatto, C.R. Natoli, A. Bianconi, J. Garcia, A. Marcelli, M. Fanfoni, I. Davoli, *Phys. Rev. B* **34**, 5774 (1986).

[58] M. Benfatto, Y. Joly, C.R. Natoli, *Phys. Rev. Lett.* **83**, 636 (1999).

[59] J.-S. Kang, H. Han, B.W. Lee, C.G. Olson, S.W. Han, K.H. Kim, J.I. Jeong, J.H. Park, B.I. Min, *Phys. Rev. B* **64**, 24429 (2001).

[60] T. Saitoh, M. Nakatake, A. Kakizaki, H. Nakajima, O. Morimoto, Sh. Xu, Y. Moritomo, N. Hamada, Y. Aiura, *Phys. Rev. B* **66**, 35112 (2002).

[61] I.S. Elfimov, V.I. Anisimov, G.A. Sawatzky, *Phys. Rev. Lett.* **82**, 4264 (1999).

[62] M.S. Moreno, J.E. Gayone, M. Abbate, A. Caneiro, D. Niebieskikwiat, R.D. Sanchez, A. de Siervo, R. Landers, G. Zampieri, *Phys. B* **320**, 43 (2002).

[63] J. Garcia, G. Subias, *J. Phys., Condens. Matter* **16**, R145 (2004).

[64] M.P. Pasternak, W.M. Xu, G.Kh. Rozenberg, R.D. Taylor, R. Jeanloz, *J. Magn. Magn. Mater.* **265**, L107 (2003).

[65] J. Gopalakrishnan, A. Chattopadhyay, S.B. Ogale, T. Venkatesan, R.L. Greene, *Phys. Rev. B* **62**, 9538 (2000).

[66] S. Nakamura, M. Tanaka, H. Kato, Y. Tokura, *J. Phys. Soc. Japan* **72**, 424 (2003).

[67] H. Ebert, G. Schütz, *Spin-Orbit Influenced Spectroscopies of Magnetic Solids*, Springer, Berlin 1996.

[68] B.T. Thole, P. Carra, F. Sette, G. van der Laan, *Phys. Rev. Lett.* **68**, 1943 (1992).

[69] P. Carra, B.T. Thole, M. Altarelli, X. Wang, *Phys. Rev. Lett.* **70**, 694 (1993).

[70] R. Felix-Medina, J. Dorantes-Dévila, G.M. Pastor, *Phys. Rev. B* **67**, 094430 (2003).